A novel rare earth zinc germanide, $Y b_2Zn_3Ge_{3.1}$; crystal structure and physical properties

2005 J. Phys.: Condens. Matter 17 385

(http://iopscience.iop.org/0953-8984/17/2/013)

INSTITUTE OF PHYSICS PUBLISHING JOURNAL OF PHYSICS: CONDENSED MATTER

J. Phys.: Condens. Matter **17** (2005) 385–397 doi:10.1088/0953-8984/17/2/013

A novel rare earth zinc germanide, $Yb_2Zn_3Ge_{3.1}$; crystal structure and physical properties

A Grytsiv[1], D Kaczorowski[2], P Rogl[1,6], V Tran[2], C Godart[3,4], K Gofryk[2] and G Giester[5]

[1] Institut für Physikalische Chemie, Universität Wien, Währingerstrasse 42, A-1090 Wien, Austria
[2] W Trzebiatowski Institute of Low Temperature and Structure Research, Polish Academy of Sciences, P-50-950 Wrocław, PO Box 1410, Poland
[3] CNRS-UPR209, ISCSA, 2-8 rue Henri Dunant, F94320 Thiais, France
[4] LURE, CNRS, Université Paris Sud, 91405 Orsay, France
[5] Institut für Mineralogie und Kristallographie, Universität Wien, Althanstrasse 14, A-1090 Wien, Austria

E-mail: peter.franz.rogl@univie.ac.at

Received 4 November 2004, in final form 29 November 2004
Published 20 December 2004
Online at stacks.iop.org/JPhysCM/17/385

Abstract

A novel ternary structure type has been determined from single crystals of $Yb_2Zn_3Ge_{3.1}$ grown from zinc flux solvent. $Yb_2Zn_3Ge_{3.1}$ crystallizes in a novel monoclinic structure type ($a = 1.5804(2)$ nm, $b = 0.429\,70(1)$ nm, $c = 1.1524(1)$ nm; $\beta = 126.14(1)^\circ$) with space group $C2/m$, $Z = 4$. The large ytterbium atoms are at the centres of pentagonal pyramids formed by Zn/Ge atoms. Zinc atoms are centred in distorted triangular prisms and polyhedra around germanium atoms are related to octahedra. The void at the centre of the Zn octahedra is only partially (20%) filled by Ge atoms. There are two positions for Yb atoms in the unit cell, which contain ions with valency slightly higher than 2+, as evidenced by x-ray absorption spectroscopy and bulk magnetic measurements. The compound exhibits metallic-like electrical conductivity, and its Seebeck coefficient shows a temperature variation characteristic of metals, being, however, fairly enhanced, as expected for intermediate valence systems.

1. Introduction

Little is known on the potentially beneficial and combined alloying influence of rare earth metals and germanium on zinc. Whilst novel rare earth (RE) zinc based alloys reveal wear-resisting properties superior to those of bronze [1], germanium is well known as an oxide

[6] Author to whom any correspondence should be addressed.

layer removing wetting agent in zinc/tin based solders [2]. Metallurgical effects such as precipitation hardening particularly require a profound knowledge of the multi-component phase equilibria and crystal structures of compounds in equilibrium with the Zn-rich solid solution. Considering ternary phase equilibria (isothermal RE–Zn–Ge sections) as basic building units, knowledge is only revealed for {Ce, Nd, Gd}–Zn–Ge systems at 600 °C [3–5]. Although these systems contain a series of ternary compounds, the crystal structures of many of them remain unknown. Structure types have hitherto been elucidated in a few cases, such as for {La, Ce, Pr, Nd, Sm, Gd}$_2$Zn$_6$Ge$_3$ ($Ce_2Zn_6Ge_3$ type) [6], {Gd, Tm, Lu}$_4$Zn$_5$Ge$_6$ ($Gd_4Zn_5Ge_6$ type) [7], {La, Ce, Pr, Nd, Sm}Zn$_{1.5}$Ge$_{0.5}$ [8] and GdZnGe (AlB_2 type) [5], GdZn$_{1.6}$Ge$_{0.6}$ and NdZnGe (Fe_2P type) [5], EuZn$_2$Ge$_2$ ($CaBe_2Ge_2$ type) [9–11], YbZn$_2$Ge$_2$ ($BaAl_4$ type) [9–11], EuZnGe (ZrBeSi type) [12], YbZnGe ($CeCu_2$ type) [12], {Ce, Nd}$_2$Zn$_{15}$Ge$_2$ (Th_2Zn_{17} type) [4, 13], CeZn$_{1.8}$Ge$_{1.2}$ (Cu_3Au type) [4], CeZn$_{1.3}$Ge$_{0.7}$ ($ThSi_2$ type) [4] and {Ce, Gd}$_4$Zn$_8$Ge$_{11-x}$ ($Ce_4Zn_8Ge_{11-x}$ type) [5, 4]. Besides the desired knowledge of phase equilibria, there is general interest in the crystal structures and physical (particularly thermoelectric) properties of those compounds, which contain rare earth elements prone to valence instabilities: Ce, Eu, Yb. We recently reported on the interesting magnetic and electric properties of {La, Ce, Pr, Nd, Sm, Gd}$_2$Zn$_6$Ge$_3$ [6]. In the search for a corresponding Yb-containing compound we obtained single crystals of an unknown phase '$Yb_2Zn_3Ge_3$'—the evaluation of its crystal structure and the characterization of its physical properties became the subject of the present paper.

2. Experimental details

Due to the low melting and boiling point of zinc metal ($T_m = 419.6$ °C, $T_b = 907$ °C [14]), synthesis of zinc-containing single-phase materials is difficult to achieve via high frequency or arc melting techniques. Employing low melting point flux solvents such as zinc, gallium, indium and mixtures thereof, the Lebeau method [15] proved to be a successful alternative for the growth of sizable single-crystal silicides and germanides [6, 9, 10, 16, 17]. In our case a Zn-rich flux appeared most suitable.

The starting materials used were zinc granules, p.A., 99.9% pure ingots of ytterbium, and Ge pieces, 99.999%. Single crystals of '$Yb_2Zn_3Ge_3$' were grown from pure zinc flux taken in a mass ratio of 7:1 with an elemental mixture of 33.3Yb–66.7Ge (at.%). Pieces of elements were contained in Al_2O_3 crucibles and vacuum sealed within thick walled quartz tubes. A typical experiment started from room temperature with a heating rate of 75 °C h^{-1} up to 1100 °C with an intermediate hold for 1 h at a temperature of 450 °C, well above the melting point of the flux. After a soaking period of 3 h, cooling to 800 °C proceeded at a speed of 25 °C h^{-1} after which the ampoules were simply removed from the hot furnace. The zinc flux was dissolved in dilute HCl. The retained crystals were significantly attacked by acid and served in a first step to elucidate the main features of the structure.

After details of the composition were established from this preliminary structure refinement, we prepared bulk material for physical property measurements. The compacted powder blend of the initial powders (Yb and Zn were powdered under cyclohexane) was sealed in evacuated silica ampoules and heat treated at 350–400 °C for four days, after which a fine powder of nearly single-phase '$Yb_2Zn_3Ge_3$' was obtained. It was re-compacted and sintered again at 850 °C for 6 h to yield a dense single-phase material suitable for physical property measurements. Contents of secondary phases (typically Zn and/or Ge) were examined by means of quantitative x-ray powder Rietveld refinement and found not to exceed 3 vol%. The composition was determined via electron probe microanalyses (EPMA) using a Carl Zeiss DSM 962 equipped with a Link EDX system operated at 20 kV and 60 μA comparing the

emissions (Yb Mα, Ge Kα and Zn Kα) for the three elements in the alloys with those from the pure elements.

For the growth of perfect single crystals for x-ray structure determination, 0.35 g of the polycrystalline sample were placed in an alumina crucible sealed in an evacuated silica ampoule and heated to 1100 °C. After a dwell period of 24 h, cooling to 900 °C proceeded at a speed of 50 °C h^{-1}, after which the sample was kept at this temperature for three days prior to final quenching; i.e., the ampoule with the sample was simply removed from the hot furnace. Well-shaped single crystals were mechanically separated and used for final structure determination.

X-ray examination of polycrystalline materials was performed at room temperature in a Guinier–Huber x-ray camera with an image plate recording system (Cu Kα_1) employing an internal standard of 99.9999 mass% pure Si (a_{Si} = 0.543 1065 nm). For Rietveld refinements we employed the FULLPROF program [18]. Inspection on an AXS-GADDS texture goniometer assured us of the high crystal quality, unit cell dimensions and Laue symmetry of the specimens prior to x-ray intensity data collection on a four-circle Nonius Kappa diffractometer equipped with a CCD area detector employing graphite monochromated Mo Kα radiation (λ = 0.071 073 nm). The orientation matrix and unit cell parameters for a monoclinic system were derived using the program DENZO [19]. No special absorption corrections were necessary because of the rather regular crystal shape and small dimensions of the specimens investigated. The structure was determined and refined with the aid of the SHELXS-97, SHELXL-97 programs [20].

X-ray absorption spectra (for taking the L_{III}-edge data) were collected at the French synchrotron radiation facility (LURE) in Orsay using the x-ray beam of the DCI storage ring (working at 1.85 GeV and ~320 mA) on the EXAFS D21 station. A double Si 311 crystal was used as a monochromator. The rejection of third-order harmonics was achieved with the help of two parallel mirrors adjusted to cut off energies higher than ~12 keV. Experiments were carried out in the energy range 8860–9040 eV, which contains the L_{III} edge of Yb. Finely powdered samples were spread on an adhesive Kapton tape and four such tapes were stacked together for preparing a sample layer of sufficient thickness to ensure a good signal.

Measurements of the various bulk properties were carried out with a series of standard techniques; details were already given in [21].

3. Results and discussion

3.1. The crystal structure of $Yb_2Zn_3Ge_{3.1}$

Systematic extinctions, only observed for C centring of the monoclinic unit cell, are compatible with several space groups, of which $C2/m$ is the one with the highest crystal symmetry. The atom arrangement was found employing direct methods with the program SHELXS-97. The search for missing symmetry (program: PLATON) confirmed space group $C2/m$ with the highest possible symmetry with all atoms adopting 4i site symmetry $(x, 0, z)$. In view of the known difficulties of distinguishing Zn and Ge atoms by x-ray diffraction techniques, balanced thermal displacement factors and interatomic distances in agreement with the sum of the metal radii (R_{Zn} = 0.1394 nm, R_{Ge} = 0.1369 nm for CN = 12) were used to locate the slightly smaller Ge atoms. Thus a fully ordered atom arrangement is obtained for the formula '$Yb_2Zn_3Ge_3$' in good agreement with the fairly single-phase bulk samples prepared from the elements, and with the composition 25.3Yb–37.6Zn–37.9Ge (at.%) controlled by means of EPMA. Consistency also exists for the lattice parameters of bulk alloys and the single-crystal specimens. Occupancies of all crystallographic sites were refined but did not reveal any

significant deviations from stoichiometry. Refining anisotropic thermal displacement factors at this stage yielded an *R*-value as low as 0.03. The routine search for possible voids in the structure revealed one position (site 2c) at the centre of an octahedron $Zn1_2Zn2_4$ with an internal radius of ∼0.13 nm. Checking for residual electron density in the structure from difference Fourier syntheses indeed revealed a small but significant value of about 18×10^{-3} e nm^{-3} corresponding to an atom in site 2c with ordering number between 5 and 7. At this point a second technique of preparation was employed to synthesize single crystals via melting the bulk material within an alumina crucible sealed in a silica tube. Refinement of one of these single crystals yielded within standard deviations the same parameter set, as well as an identical electron density in the 2c site. Wet chemical microanalyses of the bulk sample with respect to carbon and nitrogen, as well as oxygen, yielded very low carbon (0.025 mass%), nitrogen (0.02 mass% N), oxygen (0.22 mass%), sulfur (less than 0.01 mass%) and hydrogen contents (0.02 mass% H) all not exceeding background values. In order to match the residual density, a final structure refinement included a partial occupancy of germanium atoms in the 2c sites and involving all parameters yielded an *R*-value as low as 0.021 with quite reasonable atomic thermal displacement parameters on all sites, thus confirming the structure model. Results of the structure determination by means of x-ray single-crystal and powder diffractions are compared in table 1. It should be noted that refinement of the x-ray powder intensities agrees perfectly on the coordinates and atom distribution at all 4i sites obtained for single crystals; the small electron density at the 2c site, however, was detected neither by means of Rietveld refinements of the diffraction data collected from the sintered polycrystalline sample nor by means of those for re-powdered crystals grown from Zn flux. The resolution of x-ray powder diffraction techniques is too low for such a complicated structure of low symmetry.

The structure of $Yb_2Zn_3Ge_{3.1}$ is presented in figure 1(a) in a view along the [010] axis. Coordination polyhedra around atoms are shown in figure 1(b) in a three-dimensional view. Due to the low overall crystal symmetry, all coordination figures around the individual atoms in $Yb_2Zn_3Ge_{3.1}$ are rather irregular. Whilst the large ytterbium atoms, Yb1 and Yb2, are surrounded by 16 and 17 atoms, respectively, the coordination numbers of Zn and Ge atoms range between 10 and 11 for Zn atoms and 9 and 8 for Ge atoms (table 1, figure 1(b)). Ytterbium atoms are coordinated by Zn/Ge pentagonal pyramids with centring of the lateral faces. Polyhedra around the zinc atoms are usually distorted triangular prisms and polyhedra around germanium atoms are related to octahedra. Interatomic distances (see table 1) agree well with the metallic radii of pure elements.

Despite the low symmetry, the $Yb_2Zn_3Ge_{3.1}$ structure contains rather regular structure units. Particularly notable is the Yb sublattice, which contains fragments of the AlB_2 type (figure 1(a)). These triangular prisms are centred by Ge1 atoms and two $Ge_1[Yb1_2Yb2_4]$ polyhedra are linked by four Yb2 atoms. The resulting cell corresponds to the AlB_2-type lattice, where four additional Zn atoms centre the lateral faces of this unit. A slight distortion of the $[Yb1_2Yb2_4]$ triangular prisms is observed in as far as the bond lengths between Yb atoms in the *ab* plane vary from 0.3677 to 0.3898 nm, and the distance between Yb atoms in the *y* direction corresponds to the *b* lattice parameter of the $Yb_2Zn_3Ge_{3.1}$ compound ($b = 0.4297$ nm). One can see that these values are very close to the lattice parameters of rare earth germanides with AlB_2-type related structures. Close inspection of the coordination figures in the $Yb_2Zn_3Ge_{3.1}$ structure shows that the next nearest coordination of Ge2 and Ge4 atoms is formed by octahedra of Zn atoms, shown in figure 1 and listed in table 1. The octahedra $Ge2[Zn1_2Zn2_1Yb1_2Yb1_1]$ are linked by Yb atoms, and in combination with $Ge4[Zn2_4Zn1_2]$ form an infinite chain in the *ab* plane. A puzzling situation is observed for atoms forming the $Ge4[Zn2_4Zn1_2]$ octahedra, which reveal high anisotropy of the atom temperature displacement parameters (see table 1). Both single crystals investigated (one grown from Zn flux and one selected from the polycrystalline

Table 1. X-ray diffraction data for $Yb_2Zn_3Ge_{3.1}$, space group $C2/m$; No 12. (Notes: data collected with a Nonius Kappa CCD; Mo Kα; redundancy <5; $D_x = 30$ mm; RT; scan width 2° /frame. Crystal structure data were standardized using the program Typix [22].)

Parameter/compound	Single-crystal $Yb_2Zn_3Ge_{3.1}$	Powder diffraction $Yb_2Zn_3Ge_3$
Crystal size	$56 \times 56 \times 56\ \mu m^3$	—
a; b; c (nm); β (deg)	$a = 1.5804(2)$; $b = 0.429\,70(1)$ $c = 1.1524(1)$; $\beta = 126.14(1)$	$a = 1.577\,06(1)$; $b = 0.428\,957(3)$; $c = 1.150\,316(8)$; $\beta = 126.1127(3)$
ρ_x (Mg m^{-3}); μ_{abs} (mm^{-1})	8.07; 54.39	
Data collection, 2Θ range (deg); Kα	$2 \leqslant 2\Theta \leqslant 72.5$; Mo K$\alpha_{1,2}$	$24.5 \leqslant \Theta \leqslant 100$; Cu K$\alpha_1$
Total number of frames	75 s/frame; 477 frames; 9 sets	—
Reflections in refinement	$1522 \geqslant 4\sigma(F_o)$ of 1661	384
Mosaicity	<0.45	—
Number of variables	55	36
$R_F^2 = \sum \lvert F_o^2 - F_c^2 \rvert / \sum F_o^2$	0.021	$R_F = \sum \lvert F_o - F_c \rvert / \sum F_o = 0.048$
R_{Int}	0.048	$R_I = \sum \lvert I_o - I_c \rvert / \sum I_o = 0.058$
w_{R2}	0.051	$R_P = \sum \lvert y_{oi} - y_{ci} \rvert / \sum y_{oi} = 0.063$
Goodness of fit (GOF)	1.134	$R_{wP} = [\sum w_i \lvert y_{oi} - y_{ci} \rvert^2 / \sum w_i \lvert y_{oi} \rvert^2]^{1/2} = 0.092$
Extinction (Zachariasen)	0.001 20(5)	$\chi^2 = (R_w/R_e)^2 = 17.4$ $R_e = 2.22$
Yb1 at 4i $(x, 0, z)$;	$x = 0.263\,81(2)$; $z = 0.670\,09(3)$	$x = 0.263\,64(7)$; $z = 0.6702(1)$
Occ.	1.0(1)	1.00
U_{11}; U_{22}; U_{33};	0.0079(1); 0.0088(1); 0.0065(1)	$B = 0.43(2)$
U_{13}; $U_{12} = U_{23} = 0.0$	0.0036(1)	
Yb2 at 4i $(x, 0, z)$;	$x = 0.434\,15(2)$; $z = 0.088\,61(3)$	$x = 0.434\,46(8)$; $z = 0.0886(1)$
Occ.	1.0(1)	1.00
U_{11}; U_{22}; U_{33}	0.0094(1); 0.0065(1); 0.0094(1)	$B = 0.28(4)$
U_{13}; $U_{12} = U_{23} = 0.0$	0.0066(1)	
Zn1 at 4i $(x, 0, z)$;	$x = 0.062\,40(7)$; $z = 0.329\,19(9)$	$x = 0.0624(2)$; $z = 0.3315(2)$
Occ.	1.0(1)	1.00
U_{11}; U_{22}; U_{33}	0.0221(4); 0.0091(4); 0.0088(3)	$B = 0.77(5)$
U_{13}; $U_{12} = U_{23} = 0.0$	0.0058(3)	
Zn2 at 4i $(x, 0, z)$;	$x = 0.422\,79(7)$; $z = 0.358\,30(9)$	$x = 0.4236(2)$; $z = 0.3587(2)$
Occ.	1.0(1)	1.00
U_{11}; U_{22}; U_{33}	0.0123(3); 0.0380(5); 0.0096(3)	$B = 0.80(5)$
U_{13}; $U_{12} = U_{23} = 0.0$	0.0064(3)	
Zn3 at 4i $(x, 0, z)$;	$x = 0.233\,12(6)$; $z = 0.098\,40(8)$	$x = 0.2344(2)$; $z = 0.0991(2)$
Occ.	1.0(1)	1.00
U_{11}; U_{22}; U_{33}	0.0079(3); 0.0110(3); 0.0137(3)	$B = 0.78(5)$
U_{13}; $U_{12} = U_{23} = 0.0$	0.0056(3)	
Ge1 at 4i $(x, 0, z)$;	$x = 0.084\,89(5)$; $z = 0.123\,19(7)$	$x = 0.0851(2)$; $z = 0.1224(2)$
Occ.	1.0(2)	1.00
U_{11}; U_{22}; U_{33}	0.0063(2); 0.0093(3); 0.0058(2);	$B = 0.31(4)$
U_{13}; $U_{12} = U_{23} = 0.0$	0.0028(2)	
Ge2 at 4i $(x, 0, z)$;	$x = 0.378\,23(5)$; $z = 0.534\,40(7)$	$x = 0.3776(1)$; $z = 0.5344(2)$
Occ.	1.0(2)	1.00
U_{11}; U_{22}; U_{33}	0.0102(3); 0.0070(3); 0.0078(3)	$B = 0.44(5)$
U_{13}; $U_{12} = U_{23} = 0.0$	0.0058(2)	
Ge3 at 4i $(x, 0, z)$;	$x = 0.153\,46(5)$; $z = 0.820\,84(7)$	$x = 0.1538(1)$; $z = 0.8207(2)$
Occ.	1.0(2)	1.00
U_{11}; U_{22}; U_{33}	0.0111(3); 0.0075(3); 0.0114(3)	$B = 0.35$ (4)
U_{13}; $U_{12} = U_{23} = 0.0$	0.0082(2)	

Table 1. (Continued.)

Parameter/compound	Single-crystal $Yb_2Zn_3Ge_{3.1}$			Powder diffraction $Yb_2Zn_3Ge_3$	
Ge4 in 2c (0, 0, 1/2); Occ.	0.192(6)			—	
U_{11}; U_{22}; U_{33}	0.011(2); 0.0075(6); 0.009(2)			—	
U_{13}; $U_{12} = U_{23} = 0.0$	0.0082(2)			—	
Residual density; max.; min.	2.52; −2.90				
Principal mean square atomic displacements U_{ij}	Yb1	0.0092	0.0088	0.0064	
	Yb2	0.0101	0.0068	0.0065	
	Zn1	0.0283	0.0096	0.0076	
	Zn2	0.0380	0.0126	0.0093	
	Zn3	0.0154	0.0110	0.0077	
	Ge1	0.0093	0.0079	0.0055	
	Ge2	0.0102	0.0070	0.0069	
	Ge3	0.0102	0.0042	0.0042	
	Ge4	0.0667	0.0111	0.0086	
Interatomic distances <0.400 00 nm; standard deviations generally <0.000 08 nm					
CN = 16	Yb1–2 Ge2	0.299 48		Yb1–2 Ge2	0.298 69
	1 Ge2	0.300 84		1 Ge2	0.299 66
	2 Ge1	0.304 79		2 Ge1	0.304 53
	1 Ge3	0.310 39		1 Ge3	0.308 75
	1 Zn1	0.328 90		1 Zn1	0.326 75
	2 Zn3	0.340 34		2 Zn3	0.339 81
	1 Ge4	0.340 38		1 Ge4	0.339 48
	2 Zn1	0.348 33		2 Zn1	0.349 15
	2 Zn2	0.350 44		2 Zn2	0.350 33
	1 Yb2	0.385 52		1 Yb2	0.384 64
	1 Yb2	0.389 80		1 Yb2	0.389 08
CN = 17	Yb2–2 Ge3	0.305 37		Yb2–2 Ge3	0.305 06
	2 Ge1	0.305 44		2 Ge1	0.305 58
	2 Zn3	0.308 68		2 Zn3	0.309 45
	2 Zn1	0.312 75		2 Zn1	0.313 57
	2 Ge1	0.313 00		2 Ge1	0.311 51
	1 Zn2	0.321 71		1 Zn2	0.321 09
	1 Zn3	0.324 49		1 Zn3	0.322 27
	1 Ge2	0.353 15		1 Ge2	0.352 71
	1 Ge3	0.361 30		1 Ge3	0.360 69
	1 Yb2	0.367 66		1 Yb2	0.366 00
	1 Yb1	0.385 52		1 Yb1	0.384 64
	1 Yb1	0.389 80		1 Yb1	0.389 08
CN = 10	Zn1–2 Ge2	0.249 55		Zn1–2 Ge2	0.248 08
	1 Ge1	0.259 94		1 Ge1	0.263 22
	1 Ge4	0.267 14		1 Ge4	0.264 08
	1 Ge3	0.276 95		1 Ge3	0.276 66
	2 Yb2	0.312 75		2 Yb2	0.313 57
	1 Yb1	0.328 90		1 Yb1	0.326 75
	2 Yb1	0.348 33		2 Yb1	0.349 15
CN = 11	Zn2–1 Ge2	0.250 98		Zn2–1 Ge2	0.251 78
	2 Ge4	0.253 39		2 Ge4	0.252 69
	1 Ge2	0.261 38		1 Ge2	0.260 71
	1 Zn2	0.268 73		1 Zn2	0.267 22
	1 Zn3	0.271 41		1 Zn3	0.270 51
	2 Ge3	0.271 93		2 Ge3	0.271 65

Table 1. (Continued.)

Parameter/compound	Single-crystal $Yb_2Zn_3Ge_{3.1}$		Powder diffraction $Yb_2Zn_3Ge_3$	
	1 Yb2	0.321 71	1 Yb2	0.321 09
	2 Yb1	0.350 44	2 Yb1	0.350 33
CN = 10	Zn3–1 Ge1	0.252 19	Zn3–1 Ge1	0.252 18
	2 Ge3	0.259 36	2 Ge3	0.257 73
	1 Ge3	0.265 78	1 Ge3	0.266 00
	1 Zn2	0.271 41	1 Zn2	0.270 51
	2 Yb2	0.308 68	2 Yb2	0.309 45
	1 Yb2	0.324 49	1 Yb2	0.322 77
	2 Yb1	0.340 34	2 Yb1	0.339 81
CN = 9	Ge1–1 Ge1	0.25048	Ge1–1 Ge1	0.249 49
	1 Zn3	0.252 19	1 Zn3	0.252 18
	1 Zn1	0.259 94	1 Zn1	0.263 22
	2 Yb1	0.304 79	2 Yb1	0.304 53
	2 Yb2	0.305 44	2 Yb2	0.305 06
	2 Yb2	0.313 00	2 Yb2	0.311 51
CN = 8	Ge2–2 Zn1	0.249 55[a]	Ge2–2 Zn1	0.248 08[a]
	1 Zn2	0.250 98[a]	1 Zn2	0.251 78[a]
	1 Zn2	0.261 38	1 Zn2	0.260 71
	2 Yb1	0.299 48[a]	2 Yb1	0.298 69[a]
	1 Yb1	0.300 84[a]	1 Yb1	0.299 66[a]
	1 Yb2	0.353 15	1 Yb2	0.352 71
CN = 9	Ge3–2 Zn3	0.259 36	Ge3–2 Zn3	0.257 73
	1 Zn1	0.265 78	1 Zn1	0.295 96
	2 Zn2	0.271 96	2 Zn2	0.271 65
	1 Zn1	0.276 95	1 Zn1	0.276 66
	2 Yb2	0.305 37	2 Yb2	0.305 58
	1 Yb1	0.310 39	1 Yb1	0.308 75
CN = 8	Ge4 4 Zn2	0.253 39[a]	Ge4 4 Zn2	0.252 69[a]
	2 Zn1	0.26714[a]	2 Zn1	0.264 08[a]
	2 Yb1	0.340 38	2 Yb1	0.339 48

[a] Atoms marked are included in octahedra around Ge2 and Ge4 atoms; see also figure 1(b).

bulk alloy) show this feature. Attempts to solve this problem by reduction of the symmetry to *Cm* and *C*2 were unsuccessful. A likely answer to this problem lies in the partial Ge occupancy in the 2c sites (20%) that centre the $[Zn2_4Zn1_2]$ octahedra. Thus the real crystal comprises unit cells with empty $[Zn2_4Zn1_2]$ octahedra and others filled with Ge atoms. It is therefore reasonable to assume that unfilled $[Zn2_4Zn1_2]$ polyhedra exhibit a smaller size than filled Ge4$[Zn2_4Zn1_2]$ polyhedra, and this difference results in the observed anisotropy of the temperature displacement parameters of the atoms involved.

3.2. Physical properties

3.2.1. X-ray absorption. The Yb L_{III}-edge spectra of $Yb_2Zn_3Ge_{3.1}$ taken at 300 K are shown in figure 2. The peak at ≈8943 eV corresponds to the $4f^{13}(Yb^{3+})$ configuration and the peak at ≈8935 eV corresponds to the $4f^{14}(Yb^{2+})$ configuration. After subtracting the background in a standard manner, the edge was decomposed into a pair of Lorentzians (L1 and L2) and arctangent (AT1 and AT2) functions to provide the relative weights of the two electronic configurations [23]. This technique leads to a value of the valence of 2.3. As the multiplicities

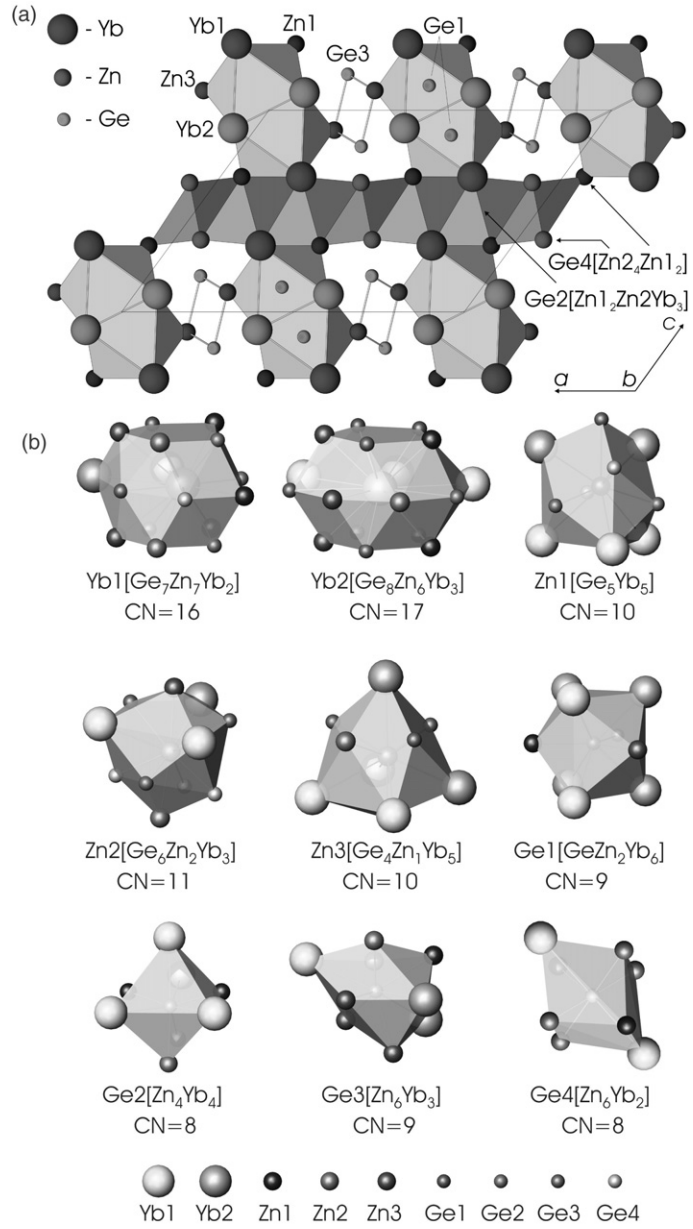

Figure 1. (a) The crystal structure of $Yb_2Zn_3Ge_{3.1}$ in a view along the [010] axis. Coordination figures around the Ge atoms are outlined. (b) The coordination of atoms in $Yb_2Zn_3Ge_{3.1}$.

of the two Yb sites are identical (4i), two possibilities are opened, i.e., the two sites are in a mixed valence state or one site has an integral valence state and the other is in a mixed valence state.

3.2.2. Magnetic behaviour. The magnetic properties of $Yb_2Zn_3Ge_{3.1}$ are summarized in figure 3. The magnetization taken at 1.9 K varies with magnetic field in a manner characteristic

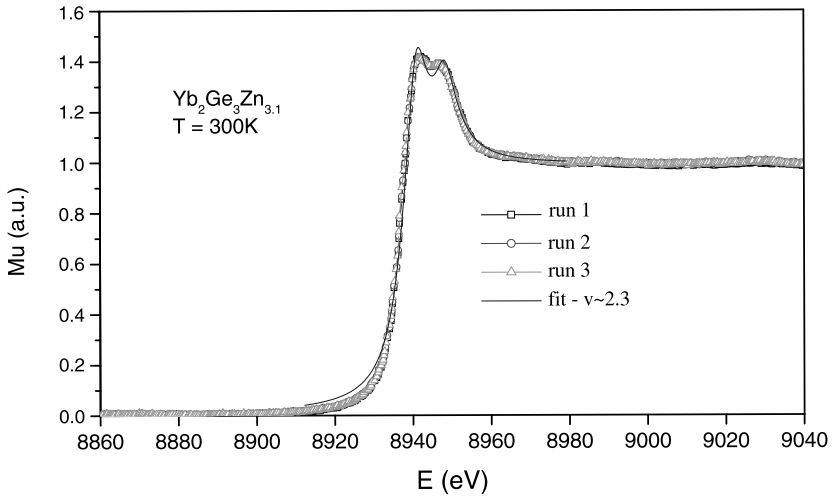

Figure 2. X-ray absorption spectra of $Yb_2Zn_3Ge_{3.1}$ at 300 K.

of paramagnets, yet its value is quite small even in the strongest fields applied. Also the magnitude of the molar magnetic susceptibility is small, and $\chi(T)$ shows a quite weak temperature dependence except for the low temperature region where a distinct upturn occurs. Apparently, the entire $\chi(T)$ curve cannot be approximated by the Curie–Weiss law, which fails especially at elevated temperatures, where a slight increase of the susceptibility with rising temperature is observed (hardly seen in figure 3), instead of a gradual decrease. In line with the hypothesis derived from the x-ray absorption data that $Yb_2Zn_3Ge_{3.1}$ contains ytterbium ions with non-integer valence, this latter effect should be attributed to a temperature-driven change in the effective population of the electronic ground state in these ions. According to the two possibilities formulated above the magnetic susceptibility of the compound studied may be described by

$$\chi(T) = \chi_{\mathrm{IV}}(T) + \chi_{\mathrm{TIP}} + \chi_{\mathrm{imp}}(T) + \chi_0 \tag{1a}$$

if only one Yb site exhibits intermediate valence character and the other contains non-magnetic Yb^{2+} ions, and alternatively by

$$\chi(T) = \chi_{\mathrm{IV}}(T) + \chi_{\mathrm{imp}}(T) + \chi_0 \tag{1b}$$

for the case of two Yb atom sites having intermediate valence (for simplicity it is assumed that the two sites have the same valence). In the above equations the term χ_0 stands for the sum of temperature independent contributions, e.g. core electron diamagnetism and conduction electron paramagnetism, χ_{TIP} represents the Pauli paramagnetism of Yb^{2+} ions and $\chi_{\mathrm{imp}}(T)$ is a Curie–Weiss-like contribution:

$$\chi_{\mathrm{imp}}(T) = \frac{C_{\mathrm{imp}}}{T - \theta_{\mathrm{imp}}} \tag{2}$$

due to the presence in the specimen for which measurements are taken of some amount of paramagnetic impurities, which could be uncompensated Yb^{3+} ions located on the sample surface or/and at grain boundaries. In turn, the susceptibility $\chi_{\mathrm{IV}}(T)$ due to intermediate valence Yb ions may be represented within the scope of the interconfiguration fluctuation

model (ICF) [24] by the formulae

$$\chi_{\mathrm{IV}}(T) = \frac{N\mu_{\mathrm{eff}}^2[1-\nu(T)]}{3k_{\mathrm{B}}(T+T_{\mathrm{sf}})}$$
$$\nu(T) = \frac{1}{1+8\exp[-E_{\mathrm{ex}}/k_{\mathrm{B}}(T+T_{\mathrm{sf}})]} \tag{3}$$

where it is assumed that the non-magnetic $4f^{14}$ ground state is separated from the magnetic $4f^{13}$ excited state by the energy E_{ex}, and the characteristic energy scale for the system is the spin fluctuation temperature T_{sf}. In the above equation the effective magnetic moment $\mu_{\mathrm{eff}} = 4.54\ \mu_{\mathrm{B}}$, $\nu(T)$ is a temperature dependent mean occupation of the ground state and the other symbols have their usual meaning.

In order to interpret the experimental results for $Yb_2Zn_3Ge_{3.1}$, the $\chi(T)$ curve was analysed in terms of equations (1)–(3). It was found that model (1*a*) cannot describe the susceptibility data for any values of the parameters, whereas model (1*b*) provides a satisfactory approximation of the experiment for the parameters $T_{\mathrm{sf}} = 679$ K, $E_{\mathrm{ex}} = 2852$ K, $C_{\mathrm{imp}} = 0.0586$ emu K mol^{-1}, $\theta_{\mathrm{imp}} = -3.5$ K and $\chi_0 \approx 0$. The least-squares fit of the data is represented in figure 3 by the thick solid curve and the contributions $\chi_{\mathrm{IV}}(T)$ and $\chi_{\mathrm{imp}}(T)$ are given by the thin solid and dashed curves, respectively. Interestingly, the values of the fitting parameters are fairly similar to those derived by the same method for binary Yb_3Ge_5 which also exhibits intermediate valence character of ytterbium ions [25]. The large magnitude of E_{ex} clearly indicates that in $Yb_2Zn_3Ge_{3.1}$ the magnetic $4f^{13}$ configuration is quite distant in energy from the non-magnetic ground state. The ICF model yields at 4.2 K the effective valence of the ytterbium atom of only 2.1. With increasing temperature the excited state becomes thermally populated and the valence increases, reaching at 800 K a value of 2.5. At $T = 300$ K the calculated effective valence is equal to 2.3, in perfect agreement with the L_{III} result (presumably just by chance, as both estimations are very crude). Finally, from the value of C_{imp} one may roughly calculate the impurity concentration: $n = C_{\mathrm{imp}}/C_{\mathrm{Yb3+}}$ ($C_{\mathrm{Yb3+}} = \mu_{\mathrm{eff}}^2/8$). This value is about 2.3 at.% Yb^{3+} ions per mole in the $Yb_2Zn_3Ge_{3.1}$ sample studied; i.e., it is far below the detection limit of the x-ray diffraction method.

3.2.3. Electrical behaviour. The electrical resistivity of $Yb_2Zn_3Ge_{3.1}$ is shown in figure 4. It reveals a metallic-like behaviour but its absolute magnitude is quite high, probably because of the porous nature of the sintered sample measured. The $\rho(T)$ curve may be reasonably well approximated by the standard Bloch–Grüneisen formula

$$\rho = \rho_0 + 4R\theta_{\mathrm{D}}\left(\frac{T}{\theta_{\mathrm{D}}}\right)^5 \int_0^{\frac{\theta_{\mathrm{D}}}{T}} \frac{x^5\,\mathrm{d}x}{(\mathrm{e}^x-1)(1-\mathrm{e}^{-x})} \tag{4}$$

with the residual resistivity $\rho_0 = 497\ \mu\Omega$ cm, the Debye temperature $\Theta_{\mathrm{D}} = 221$ K and the phonon term coefficient $R = 5.7\ \mu\Omega$ cm K^{-1}. For intermediate valence systems one expects the electrical resistivity to vary at low temperatures as T^2 [26]. As shown in the inset to figure 4, such behaviour is indeed seen for $Yb_2Zn_3Ge_{3.1}$ below about 50 K, yet for some unclear reason not at the lowest temperatures studied.

Figure 5 displays the temperature variation of the thermoelectric power of $Yb_2Zn_3Ge_{3.1}$. At room temperature the Seebeck coefficient is negative and amounts to $-12\ \mu$V K^{-1}, thus being somewhat enhanced in comparison to the values typical for conventional metals (e.g. $-1.3\ \mu$V K^{-1} for Pb or $-1.5\ \mu$V K^{-1} for Cu). With temperature decreasing from 300 K, $S(T)$ initially shows a nearly straight-line behaviour characteristic of electron thermal diffusion. Extrapolating this linear dependence to zero kelvins one finds the intercept at a rather large negative value (about $-8\ \mu$V K^{-1}), which indicates that in addition to the diffusion

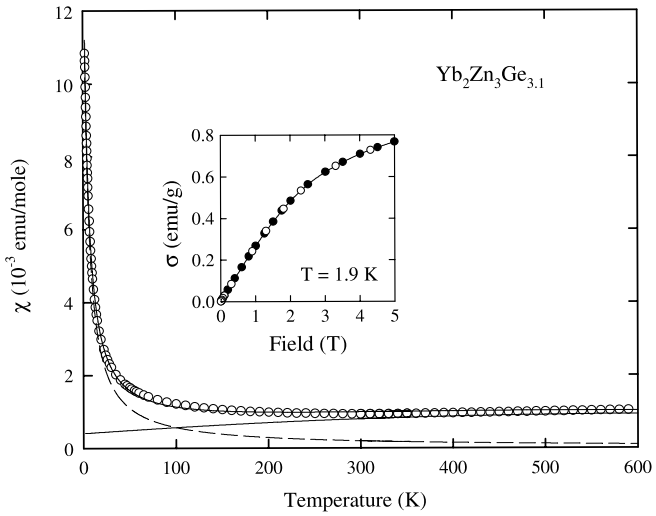

Figure 3. The temperature dependence of the molar magnetic susceptibility of $Yb_2Zn_3Ge_{3.1}$. The thick solid curve is a fit of the experimental data to equations (1)–(3). The thin solid and dashed curves represent the functions $\chi_{IV}(T)$ and $\chi_{imp}(T)$, respectively, described in the text. Inset: the magnetic field variation of the magnetization in $Yb_2Zn_3Ge_{3.1}$ taken at 1.9 K with increasing (full circles) and decreasing (open circles) field.

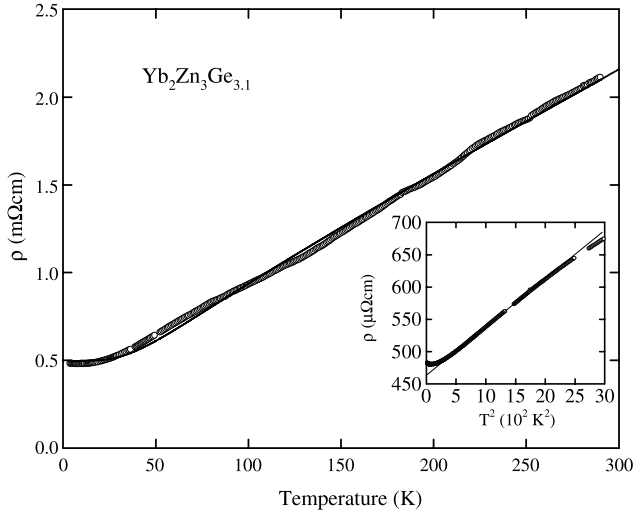

Figure 4. The temperature dependence of the electrical resistivity of $Yb_2Zn_3Ge_{3.1}$. The solid curve is a fit of the experimental data to the Bloch–Grüneisen formula. Inset: the low temperature resistivity plotted as a function of the squared temperature. The thin solid curve marks a T^2 dependence in the range 15–47 K.

thermopower there is a contribution presumably due to coupling between f and conduction electron bands. Such an effect is consistent with the intermediate valence character of the Yb ions in $Yb_2Zn_3Ge_{3.1}$. With further decreasing temperature the absolute value of the thermopower gradually rises and changes its sign to positive at about 90 K. At still lower temperatures, $S(T)$ forms a broad maximum, centred at about 30 K, and then shows a little hump near 7 K. Whereas this latter feature has no clear origin, positive low temperature maxima

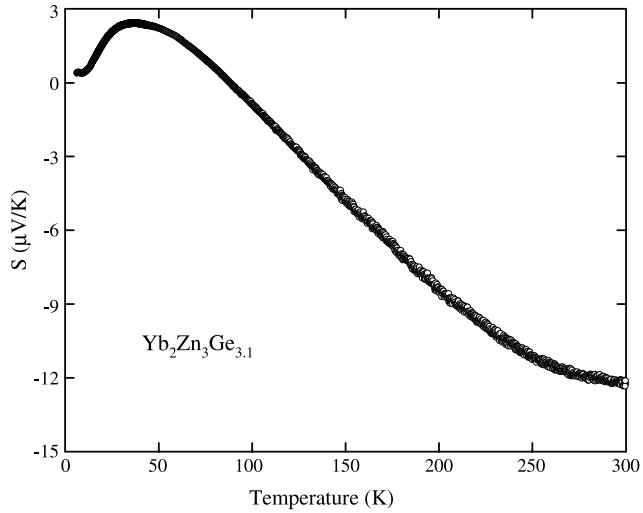

Figure 5. The temperature dependence of the thermoelectric power of $Yb_2Zn_3Ge_{3.1}$.

in $S(T)$ have been observed for Yb based materials with strong electronic correlations [28]. However, as discussed in detail in [28], this characteristic behaviour of $S(T)$ is expected for systems with low characteristic temperatures T_K and large crystal field effects [27], while for $Yb_2Zn_3Ge_{3.1}$ just the reverse is anticipated from the intermediate valence character of its magnetic susceptibility and electrical resistivity. On the other hand, the positive bump at low temperatures is known to arise from non-equilibrium phonon behaviour, the so-called phonon drag effect. This contribution to the measured thermopower increases at low temperatures as T^3 and changes as T^{-1} at higher temperatures, hence giving rise to the formation in $S(T)$ of a maximum that occurs at a temperature of 0.1–0.3 Θ_D [28]. For $Yb_2Zn_3Ge_{3.1}$ the Debye temperature Θ_D estimated from the resistivity data is about 220 K, which would indeed be consistent with the peak in $S(T)$ occurring at 30 K. Finally, it is worth mentioning that another explanation for the formation of a positive maximum in $S(T)$ followed by a linear temperature variation arises from taking into account inelastic scattering of charge carriers by acoustic phonons [29].

4. Conclusion

Single crystals of $Yb_2Zn_3Ge_{3.1}$ were grown from zinc flux. $Yb_2Zn_3Ge_{3.1}$ crystallizes in a novel monoclinic structure type ($a = 1.5804(2)$ nm, $b = 0.429\,70(1)$ nm, $c = 1.1524(1)$ nm; $\beta = 126.14(1)^\circ$) with space group $C2/m$. The large ytterbium atoms, Yb1 and Yb2, are surrounded by 16 and 17 atoms in the form of Zn/Ge pentagonal pyramids with centred lateral faces. The coordination numbers range between 10 and 11 for Zn atoms and between 9 and 8 for Ge atoms. Polyhedra around the zinc atoms are usually distorted triangular prisms and polyhedra around germanium atoms are related to octahedra. The void at the centre of the $[Zn2_4Zn1_2]$ octahedra is partially (20%) filled by Ge4 atoms. The new structure type contains fragments of AlB_2 type formed by triangular prisms of $[Yb1_2Yb2_4]$ around Ge1 atoms.

The magnetic properties of $Yb_2Zn_3Ge_{3.1}$ are governed by valence fluctuations that involve the two Yb ion sites in the crystallographic unit cell. The x-ray absorption spectroscopy as well as the bulk magnetic measurements revealed that the valency of these ions is slightly higher than 2+. The magnetic susceptibility data yield estimates for the spin fluctuation temperature of approximately 680 K and of the energy difference between the f^{14} and f^{13} states of about 2900 K.

The compound exhibits metallic character of the electrical resistivity. The fitting of the experimental data to the Bloch–Grüneisen law yields the Debye temperature of 220 K. The absolute value of the thermopower of $Yb_2Zn_3Ge_{3.1}$ is at room temperature several times larger than the value expected for a conventional metal. The overall temperature variation of the Seebeck coefficient, with a pronounced positive maximum at about 30 K, a sign change at about 90 K and a nearly linear behaviour near room temperature, may be qualitatively interpreted assuming contributions due to electron thermal diffusion, the phonon drag effect and interaction between f and conduction electron bands.

Acknowledgments

The authors are grateful to the OEAD for support within the framework of the Austrian–Polish bilateral exchange programme, project 19/2003 and the Austrian–French Amadee project 17/2003. This work was supported by the Polish State Committee for Scientific Research (grant no. 4T08A 04524).

References

[1] Li Y, Luo J, Luo Z, Xiao Z and Ngai T L 1995 *J. Mater. Process. Technol.* **55** 154
[2] Kronberg J W 1992 Solder for oxide layer-building metals and alloys *US Patent Document* 5,147,471/A, *US Patent Application* 7-681,290
[3] Salamakha P, Demchenko P, Sologub O and Bodak O 1998 *J. Alloys Compounds* **278** 227
[4] Opanych I M 1996 *PhD Chemistry Thesis* Department of Inorganic Chemistry, L'viv State University
[5] Demchenko P, Bodak O and Muratova L 2002 *J. Alloys Compounds* **339** 100
[6] Grytsiv A, Bauer E, Berger St, Hilscher G, Michor H, Paul Ch, Rogl P, Doud-Aladine A, Keller L, Roisnel T and Noël H 2003 *J. Phys.: Condens. Matter* **15** 3053
[7] Kranenberg C, Johrendt D and Mewis A 2001 *Z. Anorg. Allg. Chem.* **627** 539
[8] Rossi D and Ferro R 1996 *J. Alloys Compounds* **236** 212
[9] Grytsiv A, Leithe-Jasper A, Flandorfer H, Rogl P, Hiebl K, Godart C and Velikanova T 1998 *J. Alloys Compounds* **266** 7
[10] Grytsiv A, Kaczorowski D, Leithe-Jasper A, Rogl P, Godart C, Potel M and Noël H 2002 *J. Solid State Chem.* **163** 37
[11] Kranenberg C, Johrendt D, Mewis A, Pöttgen R, Kotzyba G, Trill H and Mosel B D 2002 *J. Solid State Chem.* **167** 107
[12] Merlo F, Pani M and Fornasini M L 1991 *J. Less-Common Met.* **171** 329
[13] Demchenko P and Bodak O 2001 *Pol. J. Chem.* **75** 153
[14] Massalski T B (ed) 1990 *Binary Alloy Phase Diagrams* 2nd edn (Materials Park, OH: ASM International)
[15] Lebeau P and Figueras J 1903 *C. R. Acad. Sci.* **136** 1329
[16] Andraka B, Pietri R, Kaczorowski D, Leithe-Jasper A and Rogl P 2000 *J. Appl. Phys.* **87** 5149
[17] Pietri R, Andraka B, Kaczorowski D, Leithe-Jasper A and Rogl P 2000 *Phys. Rev.* B **61** 12169
[18] Roisnel T and Rodriguez-Carvajal J 2001 *Mater. Sci. Forum* **378–381** 118
[19] 1998 *Nonius Kappa CCD Program Package COLLECT, DENZO, SCALEPACK, SORTAV* (Delft: Nonius)
[20] Sheldrick G M 1997 *SHELX-97, Program for Crystal Structure Refinement* (Germany: University of Göttingen) Windows version by McArdle (Galway: National University of Ireland)
[21] Grytsiv A, Rogl P, Berger St, Paul Ch, Bauer E, Godart C, Ni B, Abd-Elmeguid M M, Saccone A, Ferro R and Kaczorowski D 2002 *Phys. Rev.* B **66** 094411
[22] Parthé E, Gelato L, Chabot B, Penzo M, Cenzual K and Gladyshevskii R 1994 *TYPIX Standardized Data and Crystal Chemical Characterization of Inorganic Structure Types* (Berlin: Springer)
[23] Godart C, Achard J C, Krill G and Ravet-Krill M F 1983 *J. Less-Common Met.* **94** 177
[24] Sales B C and Wohlleben D K 1975 *Phys. Rev. Lett.* **35** 1240
[25] Grytsiv A, Kaczorowski D, Leithe-Jasper A, Rogl P, Potel M, Noël H, Pikul A P and Velikanova T 2002 *J. Solid State Chem.* **165** 178
[26] Lawrence J M, Riseborough P S and Parks R D 1981 *Rep. Prog. Phys.* **44** 1
[27] Zlatić V, Horvatić B, Milat I, Coqblin B, Czycholl G and Grenzebach C 2003 *Phys. Rev.* B **68** 104432 and references cited therein
[28] Blatt F, Schroeder P, Foiles C and Greig D 1976 *Thermoelectric Power of Metals* (New York: Plenum)
[29] Durczewski K and Ausloos M 1994 *Phys. Rev.* B **49** 13215